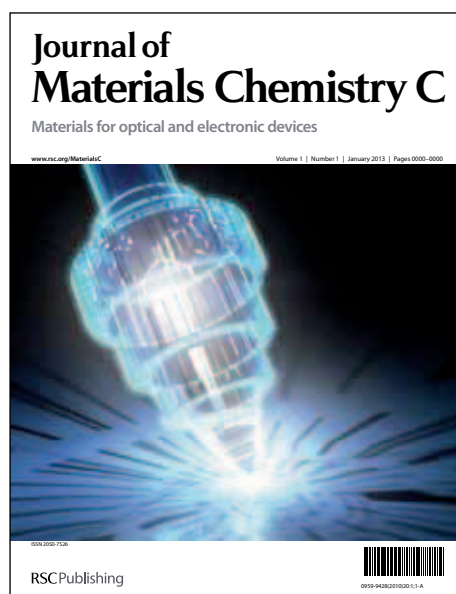


Journal of Materials Chemistry C

Accepted Manuscript



This is an *Accepted Manuscript*, which has been through the RSC Publishing peer review process and has been accepted for publication.

Accepted Manuscripts are published online shortly after acceptance, which is prior to technical editing, formatting and proof reading. This free service from RSC Publishing allows authors to make their results available to the community, in citable form, before publication of the edited article. This *Accepted Manuscript* will be replaced by the edited and formatted *Advance Article* as soon as this is available.

To cite this manuscript please use its permanent Digital Object Identifier (DOI®), which is identical for all formats of publication.

More information about *Accepted Manuscripts* can be found in the [Information for Authors](#).

Please note that technical editing may introduce minor changes to the text and/or graphics contained in the manuscript submitted by the author(s) which may alter content, and that the standard [Terms & Conditions](#) and the [ethical guidelines](#) that apply to the journal are still applicable. In no event shall the RSC be held responsible for any errors or omissions in these *Accepted Manuscript* manuscripts or any consequences arising from the use of any information contained in them.

Nanostructured Flexible Magneto-dielectrics for Radio Frequency Applications

Mert Vural,^a Benjamin Crowgey,^b Leo C. Kempel,^b and Peter Kofinas*^c

^aDepartment of Materials Science and Engineering, University of Maryland, College Park, MD 20742, USA.; E-mail:mvural@umd.edu

^bDepartment of Electrical and Computer Engineering, Michigan State University, East Lansing, MI 48824, USA.

^cFischell Department of Bioengineering, University of Maryland, College Park, MD 20742, USA.; E-mail:kofinas@umd.edu

Abstract

Flexible magneto-dielectric composites were prepared by dispersing high saturation magnetization (M_s), low coercivity (H_c), air-stable, Fe/citrate nanoparticles and heterostructures of Fe/Ag core-shell nanoparticles in an elastomer (polydimethylsiloxane) matrix. Fe/citrate nanoparticles with a polycrystalline Fe core, a thin oxide layer, and a citrate shell have a M_s of 144 emu/g and H_c of 420 Oe. Fe/Ag core-shell nanoparticles exhibit lower M_s of 98 emu/g and H_c of 210 Oe prior to annealing. The saturation magnetization of Fe/Ag core-shell nanoparticles increased to 120 emu/g and the H_c decreased to 58 Oe after annealing, due to formation of the heterostructure and changes in the chemical composition and size of the oxide layer. Magneto-dielectric composites fabricated with air-stable Fe/citrate nanoparticles possess high μ (3.0) and moderate ϵ (11.6) while maintaining low magnetic (0.29) and dielectric (0.051) loss. Moreover magneto-dielectric composites fabricated using Fe/Ag heterostructures combine high μ (2.25) and ϵ (22.3) with low magnetic (0.24) and dielectric (0.09) loss. Radio Frequency antennas made from Fe/citrate nanoparticle and Fe/Ag heterostructure composites have achieved size reductions of 44% and 38%, respectively.

Introduction

Hybrid materials with high magnetic permeability (μ) and dielectric permittivity (ϵ) known as magneto-dielectric materials are essential for the development of high efficiency microwave electronic devices and their miniaturization.¹ Polymer-magnetic nanoparticle composites have promise as magneto-dielectric hybrids, due to their low magnetic and dielectric loss, mechanical flexibility, and ease of processability. The polymer matrix prevents particle aggregation, reducing conductivity losses, and provides mechanical flexibility. Magnetic nanoparticles dispersed in a polymer matrix contribute to the permeability and permittivity of the magneto-dielectric composite.²

The permeability of polymer-magnetic nanoparticle composites is limited by magnetic resonance frequency (f_{res}) and saturation magnetization (M_s) of the magnetic nanoparticles through the Snoek Limit.³ The permeability drops significantly for frequencies above f_{res} . For this reason polymer composites containing MnZn and NiZn ferrites or similar materials with high permeability, yet low f_{res} have found limited application in microwave electronics.⁴ Additionally, materials with low M_s such as iron oxides cannot achieve sufficient permeability to be utilized for microwave device miniaturization.^{2,5}

The dielectric and magnetic loss of magneto-dielectric composites are important properties that need to be minimized in order to improve the efficiency of microwave electronic devices. Dielectric losses mostly originate from eddy currents generated in the material. The eddy current generation in polymer-magnetic nanoparticle composites can be reduced by decreasing the size of nanoparticles below a critical dimension (skin depth).⁶ It is possible to increase the skin depth of the hybrid material by decreasing the conductivity originating from the percolation of magnetic nanoparticles.⁷ As a consequence low conductivity leads to low dielectric loss. The coercivity (H_c) of magnetic nanoparticles induces magnetic losses in polymer-magnetic nanoparticle composites.⁸ Magnetic losses can be reduced without sacrificing any magnetization by the use of superparamagnetic nanoparticles. However, it is quite challenging to synthesize superparamagnetic nanoparticles with high M_s . Magnetic materials with high M_s such as ferromagnetic iron cannot maintain their magnetization at dimensions smaller than the critical superparamagnetic size because of excessive oxidation.^{9, 10} Polymer-

magnetic nanoparticle composites reported in literature consist of either oxidized superparamagnetic nanoparticles with no coercivity and low M_s , resulting in low μ , or high M_s ferromagnetic nanoparticles with substantial coercivity leading to high magnetic loss.^{2, 5, 11, 12}

In this work, we report on the fabrication of two sets of flexible magneto-dielectric composites with low magnetic and dielectric loss. This is achieved by the dispersion of high M_s , low coercivity air-stable iron (Fe) nanoparticles and iron/silver (Fe/Ag) heterostructures in polydimethylsiloxane (PDMS) matrices. The magneto-dielectric composites made of air-stable Fe/citrate nanoparticles can be adapted to the fabrication of broadband RF antennas, since they possess high μ (3), while maintaining low magnetic (0.29) and dielectric (0.051) loss.¹³ Additionally, Fe/citrate nanoparticle composites are shape compliant, allowing tensile elongation up to 15% strain before failure. Fe/Ag heterostructures formed by thermal annealing of Fe/Ag core-shell nanoparticles were dispersed in PDMS to fabricate magneto-dielectric composites with high μ (2.25) and ϵ (22.3), but low magnetic (0.24) and dielectric (0.09) loss, which makes them suitable for RF antenna miniaturization.^{1, 14} The Fe/Ag heterostructure composites are able to deform plastically under tensile elongation up to 70% strain.

Experimental

Synthesis of air-stable Fe/citrate nanoparticles

Fe/citrate nanoparticles were synthesized at room temperature from FeSO_4 using NaBH_4 as the reducing agent. $\text{FeSO}_4 \cdot 7\text{H}_2\text{O}$ (10mmol) and trisodium citrate dihydrate (2mmol) were dissolved in 2.5 L deionized water. The mixture was stirred with a magnetic stirrer for 5 minutes, then NaBH_4 (20mmol) was added to the mixture to initiate nanoparticle nucleation. The mixture was allowed to react for 20 minutes, and the nanoparticles were extracted using a rare-earth magnet for sedimentation. The particles were washed with ethanol 10 times, then vacuum dried and stored at atmospheric conditions.

Synthesis of Fe/Ag core-shell nanoparticles and heterostructures

Fe/Ag core-shell nanoparticles were synthesized at room temperature using a similar method. In this procedure Fe/citrate nanoparticles were reacted for 5 minutes instead of

20 minutes, then an aqueous AgNO_3 (7ml, 0.5M) solution was injected into the reaction. The mixture was allowed to stir for 20 minutes, and the core-shell nanoparticles were collected using magnet sedimentation. The collected particles were washed with ethanol 10 times then vacuum dried. The Fe/Ag core-shell nanoparticles were annealed at 600°C under flow of reducing gas (Argon/Hydrogen (95%, 5%)) for 1 hour to form a heterostructure of Fe/Ag core-shell nanoparticle aggregates with a coherent interface. The resulting Fe/Ag heterostructures were kept under atmospheric conditions.

Preparation of flexible magneto-dielectric composites

PDMS (Sylgard 184, Dow Corning) was prepared by mixing base silicone polymer with a curing agent in a 10:1 weight ratio. Dry Fe/citrate nanoparticles or Fe/Ag heterostructures were mixed in the polymer at the desired nanoparticle loading. The polymer particle mixture was poured into a mold, placed in a vacuum dessicator for 30 minutes to remove air bubbles, and cured at 100°C for 4 hours.

Characterization

Transmission Electron Microscope (TEM) (JEOL 2100F), Powder X-Ray Diffraction (XRD)(Bruker C2 Discover-Source: Cu-K α ($\lambda=0.154\text{nm}$)) and X-ray photoelectron spectrometer (Kratos Axis 165, Al K α (1486.6 eV)) were used for structural and elemental characterization of the nanoparticles via imaging, Energy Dispersive X-Ray Spectroscopy (EDS), Selected Area Electron Diffraction (SAED), Powder Diffraction and X-ray Photoelectron Spectroscopy (XPS). Vibrating Sample Magnetometer (VSM; Lakeshore 7400 series) was used to characterize the magnetic properties of the nanoparticles. Dynamic Mechanical Analysis (TA Instruments Q800) was used to characterize the mechanical properties of the polymer nanoparticle composites. The magnetodielectric properties of the composites were determined using an Agilent RF impedance/material analyzer (E4991A).

Results and Discussion

The TEM images and SAED patterns of air-stable Fe/citrate, Fe/Ag core-shell nanoparticles and Fe/Ag heterostructures are presented in Figure 1. The air-stable Fe/citrate nanoparticles capped with citrate developed a very thin oxide shell, which

helps prevent further oxidation of the Fe core along with the citrate capping layer (Figure 1A). The average particle size for the air-stable Fe/citrate nanoparticles was measured to be 100 nm with a standard deviation of 19 nm (100 ± 19 nm). The Fe/Ag core-shell nanoparticles also have an oxide layer similar to the Fe/citrate nanoparticles, which separates the Fe core from the shell layer consisting of Ag nanoparticles (Figure 1B). The average diameter for the Fe/Ag core-shell nanoparticles was 120 ± 23 nm, which is slightly higher than the Fe/citrate nanoparticles because of the additional Ag nanoparticles covering the Fe core. The Fe/Ag heterostructures consist of aggregates of Fe/Ag core-shell nanoparticles with the Ag shell layer forming a coherent interface upon annealing at 600°C as illustrated in Figure 1C. In addition to TEM, SAED was used to identify the crystalline structure of each sample.

The SAED pattern of Fe/citrate nanoparticles indicates a microstructure of polycrystalline body centered cubic (bcc) Fe with Debye rings that correspond to, crystallographic planes Fe (110) and Fe (211) (Figure 1A(ii)-inset). The SAED pattern of Fe/Ag core-shell nanoparticles is an overlay of the polycrystalline bcc Fe pattern on the polycrystalline Ag pattern (Figure 1B(ii)-inset). The Debye rings that represent the crystallographic planes in polycrystalline microstructure of Fe core and Ag shell are shown as an inset in Figure 1B(ii).

The crystalline structure of Fe/Ag core-shell nanoparticles changed significantly after thermal annealing under reducing gas flow. The crystal size of Ag shell increased after annealing, as inferred by the discontinuous Debye rings of Ag crystalline planes in the SAED pattern of the Fe/Ag heterostructure (Figure 1C(ii)-inset). The SAED pattern of the Fe/Ag heterostructure shows Laue diffraction patterns representing Fe crystalline planes instead of Debye rings. This indicates a significant increase in crystal size for the Fe core (Figure 1C(ii)-inset).

The average crystal size of the Fe in nanoparticles and heterostructures is an important structural parameter for the characterization and tunability of the magnetic properties (M_s , H_c) for both nanoparticles and heterostructures. Crystals below the critical superparamagnetic to ferromagnetic transition size of 10 nm for Fe result in zero coercivity.¹⁵ However, further reducing the crystal size below the critical transition size leads to a decrease in M_s .¹⁵ Powder X-Ray Diffraction (XRD) was utilized to identify the

crystalline structure and crystal size of Fe in each material (Figure 2). The average crystal size of Fe in nanoparticles and heterostructures was determined from the diffraction peak of Fe (110) plane using Scherrer's Equation.¹⁶ The XRD data indicates that the core of the nanoparticles consist of polycrystalline iron with an average crystal size of 5 nm for both Fe/citrate nanoparticles and Fe/Ag core-shell nanoparticles. Consistent with SAED patterns, the peaks of the Fe planes become sharper after annealing, which indicates an increase in crystal size. The average crystal size of Fe for the Fe/Ag heterostructures calculated from XRD data is 9.6 nm, which confirms the increase in crystal size with annealing (Figure 2).

The chemical composition of nanoparticles and heterostructures is equally important as the morphology for the displayed magnetic properties. Characterization of chemical composition for each nanoparticle and heterostructure was performed using localized EDS. XPS was used to characterize surface compositions of nanoparticles and heterostructures.

The STEM images and corresponding elemental EDS map for each nanoparticle and heterostructure are presented in Figure 3. The elemental EDS map of Fe/citrate nanoparticles shows a thin oxide layer covering the surface of the Fe core (Figure 3A). The oxide layer remains stable after being stored under ambient conditions at room temperature for 6 months (Figure S1-B). Upon annealing Fe/citrate nanoparticles with an analogous procedure for Fe/Ag core-shell nanoparticle annealing, the stable oxide layer grew thicker (Figure S1-B). The elemental EDS map of Fe/Ag core-shell shows a discontinuous shell layer formed by Ag nanoparticles around the Fe core prior to annealing (Figure 3B), consistent with the TEM images (Figure 1B). However, the EDS map does not indicate a distinct oxide shell (Figure 3B). After thermal annealing, the Fe/Ag core-shell nanoparticles form a heterostructure with an Ag shell with better coverage, as illustrated in the elemental EDS map (Figure 3C). The EDS map of the Fe/Ag heterostructure shows no obvious signs of oxidation at the surface. This can be attributed to the presence of a noble metal layer of Ag.

The characterization of the surface chemical composition of nanoparticles and heterostructures using XPS reveals the state of oxidation for Fe at the interface between the Fe core and shell layers (Figure 4). The XPS data agrees well with EDS for Fe/citrate

nanoparticles where both indicate the existence of an oxide layer covering the Fe core (Figure 4A-inset). The oxide layer apparent at TEM images of Fe/Ag core-shell nanoparticles (Figure 1B) was confirmed by XPS (Figure 4B-inset). The oxide layer was identified as Fe_2O_3 from the satellite peak appearing at 718.8 eV for both Fe and Fe/Ag core-shell nanoparticles (Figure 4(A,B)).¹⁷ The XPS data also indicates the existence of elemental Fe represented by the peak located at 706.7 eV (Figure 4(A, B)-inset). The existence of elemental Fe confirms that the oxide layer is as thin as the limited mean free path of X-rays.¹⁸

The XPS data of Fe/Ag heterostructures shows that the state of oxidation and thickness of the oxide layer has changed after annealing (Figure 4C). The oxide layer of Fe_2O_3 became Fe_3O_4 after annealing, which can be inferred by the absence of the satellite peak at 718.8 eV (Figure 4C-inset). Additionally, the elemental Fe peak became more prominent relative to the oxide related peaks ($\text{Fe}(3p_{1/2})$, $\text{Fe}(3p_{3/2})$), indicating that the oxide layer becomes thinner after annealing (Figure 4C-inset). The change in oxidation state and oxide layer thickness after annealing is consistent with previously reported Fe nanoparticles that were annealed in reducing ambient.¹⁹

The magnetic characterization correlates well with both the morphology and chemical composition of the nanoparticles and heterostructures. The Fe/citrate nanoparticles demonstrated significant M_s (144 emu/g), and high coercivity (420 Oe) (Figure 5A). The Fe/Ag core-shell nanoparticles have a lower M_s (98 emu/g) than the Fe/citrate nanoparticles, due to the non-magnetic shell layer of Ag.

The coercivity of Fe/Ag core-shell nanoparticles (210 Oe) is smaller than for Fe/citrate nanoparticles because the increase in size of the nanoparticle, reduces the influence of surface anisotropy.²⁰ The Fe/Ag heterostructures exhibit a higher M_s (120 emu/g) as compared to Fe/Ag core-shell nanoparticles (98 emu/g) due to the increase in average Fe crystal size and decrease in oxide layer thickness after annealing (Figure 5A).¹¹ The increase in Fe crystal size did not build additional coercivity because the average crystal size remained below the critical dimension for superparamagnetic to ferromagnetic transition. Moreover, the shape anisotropy became even less significant for Fe/Ag heterostructures since the size increased significantly as the Fe/Ag core-shell nanoparticles aggregate (Figure 1C). As a result, the coercivity of Fe/Ag heterostructures

decreased to 58 Oe (Figure 5A). The magnetic properties of Fe/Ag core-shell nanoparticles and Fe/Ag heterostructures were evaluated after 6 months, in order to assess the stability of the nanoparticles (Figure 5(B-C)). The M_s of the Fe/Ag core-shell nanoparticle were decreased by 24% as a result of oxidation (Figure 5B), which was confirmed by EDS studies (Figure S2). The coercivity decreased slightly to 200 Oe. The magnetic properties of Fe/Ag heterostructures remained stable over the same period as a result of the protective Ag layer preventing oxidation (Figure 5C).

The Fe/citrate nanoparticles and Fe/Ag heterostructures were dispersed in a PDMS matrix and cured to form flexible magnetodielectric composites. The mechanical stress-strain curve for each polymer/nanoparticle composite is presented in Figure 6. The Young's modulus of Fe/citrate nanoparticle (1.75 MPa) and Fe/Ag heterostructure (0.79 MPa) composites with nanoparticle loading of 50wt% is higher than the modulus of the pure PDMS elastomer (0.56 MPa), indicating good adhesion between nanoparticles and the PDMS matrix (Figure 6A).²¹ Both Fe/citrate nanoparticles and Fe/Ag heterostructure composites with 50wt% nanoparticle loading exhibit 120% tensile elongation at break (Figure 6A). The composites made of Fe/citrate nanoparticles with 75wt% nanoparticle loading can deform elastically until failure at 15% strain (Figure 6B). On the other hand composites made of Fe/Ag heterostructure composites with 75wt% nanoparticle loading can deform plastically until failure at a strain of 70%, possibly due to better adhesion between Ag and PDMS (Figure 6B).²¹ The Young's modulus of the composites increases with increasing nanoparticle loading; up to 11.1 MPa and 3.3 MPa for Fe/citrate nanoparticle and Fe/Ag heterostructure composites at 75wt% nanoparticle loading, respectively.

The electromagnetic constants (μ , ϵ) and loss characteristics of both Fe/citrate nanoparticle and Fe/Ag heterostructure composites were measured at a frequency range of 1 MHz to 8 GHz. The ϵ dispersion relation for composites of Fe/citrate nanoparticles and Fe/Ag heterostructures with 50wt% nanoparticle loading was flat at this frequency range with no sign of dielectric resonance or relaxation that could lead to additional dielectric loss ($\tan\delta_\epsilon = \epsilon''/\epsilon'$) (Figure 7A). Due to the Ag shell, the ϵ values of Fe/Ag heterostructure composite (8) is higher than ϵ of the Fe/citrate nanoparticle composite

(4.2) with the same nanoparticle loading of 50wt%.

The dielectric loss values remain low up to a frequency of 3 GHz for both Fe/citrate nanoparticle (0.04) and Fe/Ag heterostructure (0.06) composites with nanoparticle loadings of 50wt% (Figure 7B). The dielectric loss value of Fe/Ag heterostructure composites increases drastically above 3 GHz due to conductivity losses introduced by the Ag shell. The μ and magnetic loss ($\tan\delta_{\mu}=\mu''/\mu'$) dispersion relation shows a magnetic relaxation starting at 2.25 GHz for the composites with 50wt% nanoparticle loading (Figure 7(A-B)). The μ values for both Fe/citrate nanoparticle and Fe/Ag heterostructure composites are promising for RF device fabrication, reaching 1.83 and 1.55 at 1.8 GHz, respectively (Figure 7A). The magnetic loss is significantly lower for Fe/citrate nanoparticle (0.06) composites and Fe/Ag heterostructure (0.07) composites at 1.8 GHz (Figure 7B). The magnetic loss increases more drastically for Fe/citrate nanoparticle composites at higher frequencies, which is possibly due to hysteresis losses and the influence of the Ag shell on magnetic relaxation by altering interparticle interactions (Figure 7B).²²

The ϵ and dielectric loss values of the Fe/citrate nanoparticle composite with 75wt% nanoparticle loading are stable from 1 MHz to 8 GHz (Figure 7(C-D)). However, the ϵ and dielectric loss dispersion relation of the Fe/Ag heterostructure composite with 75wt% nanoparticle loading indicate a dielectric relaxation at 4.4 GHz, due to aggregation of the Fe/Ag heterostructure with increased concentration (Figure 7(C-D)).²³ As a result ϵ values decrease and the dielectric loss increases significantly for frequencies reaching 4.4 GHz. Even though the dielectric relaxation decreases ϵ and increases dielectric loss of the Fe/Ag heterostructure composites, they still possess high ϵ (22.3) and low dielectric loss (0.09) up to 3 GHz. The μ and magnetic loss dispersion relation of composites with 75wt% nanoparticle loading indicates a magnetic relaxation centered at 2.25 GHz similar to composites with 50wt% nanoparticle loading (Figure 7(C-D)). However, both Fe/citrate nanoparticle and Fe/Ag heterostructures have high μ and low magnetic loss values for frequencies lower than the magnetic relaxation frequency of 2.25 GHz. The Fe/citrate nanoparticle composites with 75wt% nanoparticle loading have μ and magnetic loss values of 3 and 0.29 at 1.8 GHz, respectively. The Fe/Ag heterostructure composites with 75wt% nanoparticle loading have a μ of 2.15 and magnetic loss of 0.24 at 1.8 GHz.

The magnetic loss remains stable for frequencies beyond the magnetic relaxation for Fe/Ag heterostructure composites unlike Fe/citrate nanoparticle composites, which tend to have higher magnetic loss with increasing frequency (Figure 7D). As the particles get more densely packed with increasing concentration, the influence of the Ag shell as a spacer becomes more influential compared to coercivity effects, thus fixing the magnetic loss of Fe/Ag heterostructures at 0.24 beyond 2.25 GHz.²² Flexible RF antennas have been fabricated using Fe/citrate nanoparticle and Fe/Ag heterostructure composites that operates at frequencies of 1.7 GHz and 1.9 GHz, respectively (Figure S3). The flexible magneto-dielectric composites fabricated using Fe/citrate nanoparticles reduced the size of the RF antenna operating at 1.7 GHz by 44%. The Fe/Ag heterostructure composite has scaled down the size of the RF antenna with an operation frequency of 1.9 GHz by 38%.

Conclusions

We have fabricated elastic magneto-dielectric composites with low loss by embedding high M_s , low H_c , air-stable magnetic nanoparticles and heterostructures in an elastomer matrix (PDMS). Fe/citrate nanoparticles and Fe/Ag heterostructures have demonstrated good adhesion with the PDMS matrix. As a result the composites with 50wt% nanoparticle loading remain flexible up to a tensile elongation of 120%. These composites demonstrated promising ϵ and μ values with low dielectric and magnetic loss, while still maintaining their flexibility. The utilization of magnetic nanoparticles with appropriate crystal size, while still protecting the magnetic core against oxidation, provide a substantial advantage regarding ϵ , μ , loss values, and tunability of material properties for various applications in the field of RF communication devices. The Fe/citrate nanoparticle composites demonstrated higher permeability and lower dielectric loss due to the absence of a highly conductive and non-magnetic Ag layer. Conversely, the Ag layer allowed Fe/Ag heterostructure composites to achieve higher permittivity, lower magnetic loss and better mechanical elasticity. The composites have reduced the size of RF patch antennas as much as 44%. We believe this simple, yet effective method for designing and processing magneto-dielectric materials with different functionalities

can have application in the construction of various communication devices for flexible RF electronics.

Acknowledgements

This work was supported by AFOSR through grant #FA95500910430. We acknowledge the support from the Nanoscale Imaging, Spectroscopy and Properties Laboratory (NISPLab) at the University of Maryland Nanocenter.

References

1. A. O. Karilainen, P. M. T. Ikonen, C. R. Simovski and S. A. Tretyakov, *Ieee T Antenn Propag*, 2011, 59, 3991-3998.
2. T. I. Yang, R. N. C. Brown, L. C. Kempel and P. Kofinas, *J Magn Magn Mater*, 2008, 320, 2714-2720.
3. J. L. Snoek, *Physica*, 1948, 14, 207-217.
4. B. D. Cullity and C. D. Graham, *Introduction to Magnetic Materials*, Hoboken: Wiley, 2009.
5. A. Caprile, M. Coisson, F. Fiorillo, P. Kabos, O. M. Manu, E. S. Olivetti, M. A. Olariu, M. Pasquale and V. A. Scarlatache, *Ieee T Magn*, 2012, 48, 3394-3397.
6. L. Z. Wu, J. Ding, H. B. Jiang, L. F. Chen and C. K. Ong, *J Magn Magn Mater*, 2005, 285, 233-239.
7. Y. Shirakata, N. Hidaka, M. Ishitsuka, A. Teramoto and T. Ohmi, *Ieee T Magn*, 2008, 44, 2100-2106.
8. C. Morales, J. Dewdney, S. Pal, S. Skidmore, K. Stojak, H. Srikanth, T. Weller and J. Wang, *Ieee T Microw Theory*, 2011, 59, 302-310.
9. F. Dumestre, B. Chaudret, C. Amiens, P. Renaud and P. Fejes, *Science*, 2004, 303, 821-823.
10. L. M. Lacroix, S. Lachaize, A. Falqui, M. Respaud and B. Chaudret, *J Am Chem Soc*, 2009, 131, 549-557.
11. T. I. Yang, R. N. C. Brown, L. CKempel and P. Kofinas, *Nanotechnology*, 2011, 22.
12. T. I. Yang, R. N. C. Brown, L. C. Kempel and P. Kofinas, *J Nanopart Res*, 2010, 12, 2967-2978.
13. S. Borah and N. S. Bhattacharyya, *Compos Part B-Eng*, 2012, 43, 1988-1994.
14. L. Yang, L. J. Martin, D. Staiculescu, C. P. Wong and M. M. Tentzeris, *Ieee T Microw Theory*, 2008, 56, 3223-3230.
15. D. L. Huber, *Small*, 2005, 1, 482-501.
16. Z. Zhang, F. Zhou and E. J. Lavernia, *Metall Mater Trans A*, 2003, 34A, 1349-1355.
17. H. S. Lim, J. W. Oh, S. Y. Kim, M. J. Yoo, S. D. Park and W. S. Lee, *Chem Mater*, 2013, 25, 3315-3319.

18. D. D. Sarma, P. K. Santra, S. Mukherjee and A. Nag, *Chem Mater*, 2013, 25, 1222-1232.
19. S. H. Sun and H. Zeng, *J Am Chem Soc*, 2002, 124, 8204-8205.
20. C. R. Vestal and Z. J. Zhang, *Nano Lett*, 2003, 3, 1739-1743.
21. A. Goyal, A. Kumar, P. K. Patra, S. Mahendra, S. Tabatabaei, P. J. J. Alvarez, G. John and P. M. Ajayan, *Macromol Rapid Comm*, 2009, 30, 1116-1122.
22. N. A. Frey, M. H. Phan, H. Srikanth, S. Srinath, C. Wang and S. Sun, *J Appl Phys*, 2009, 105.
23. Y. Shen, Y. H. Lin and C. W. Nan, *Adv Funct Mater*, 2007, 17, 2405-2410.

Figure Captions

Fig. 1 TEM image of A) Fe/citrate nanoparticles, B) Fe/Ag core-shell nanoparticles, C) Fe/Ag heterostructures. The SAED characterization of each particle is placed as an inset.

Fig. 2 Powder X-Ray Diffraction data of Fe/citrate nanoparticles, Fe/Ag core-shell nanoparticles and Fe/Ag heterostructures.

Fig. 3 Scanning Transmission Electron Microscope (STEM) image and EDS elemental map of A) Fe/citrate nanoparticles, B) Fe/Ag core-shell nanoparticles, C) Fe/Ag heterostructures.

Fig. 4 XPS spectrum of A) Fe/citrate nanoparticle, B) Fe/Ag core-shell nanoparticle and Fe/Ag heterostructures. Localized XPS spectras around the Fe2p region is shown as an inset.

Fig. 5 A) Room temperature magnetic hysteresis curves for Fe/citrate nanoparticles, Fe/Ag core-shell nanoparticles and Fe/Ag heterostructures as synthesized. Time dependent magnetic hysteresis curves for B) Fe/Ag core-shell nanoparticles, and C) Fe/Ag heterostructures. The low-field magnetization curve is shown as an inset.

Fig. 6 Mechanical Stress/Strain curves for Fe/citrate (circles) and Fe/Ag (squares) heterostructure polymer composites with A) 50wt% and B) 75wt% nanoparticle loading. The images of elongated composites are shown as an inset.

Fig. 7 A) Dielectric (ϵ), Magnetic Permeability (μ) dispersion and B) dielectric and magnetic loss values of Fe/citrate (circles) and Fe/Ag heterostructure (squares) composites with 50wt% nanoparticle loading. C) Dielectric (ϵ), Magnetic Permeability (μ) dispersion and D) dielectric and magnetic loss values of Fe/citrate (circles) and Fe/Ag heterostructure (squares) composites with 75wt% nanoparticle loading.

Figure 1:

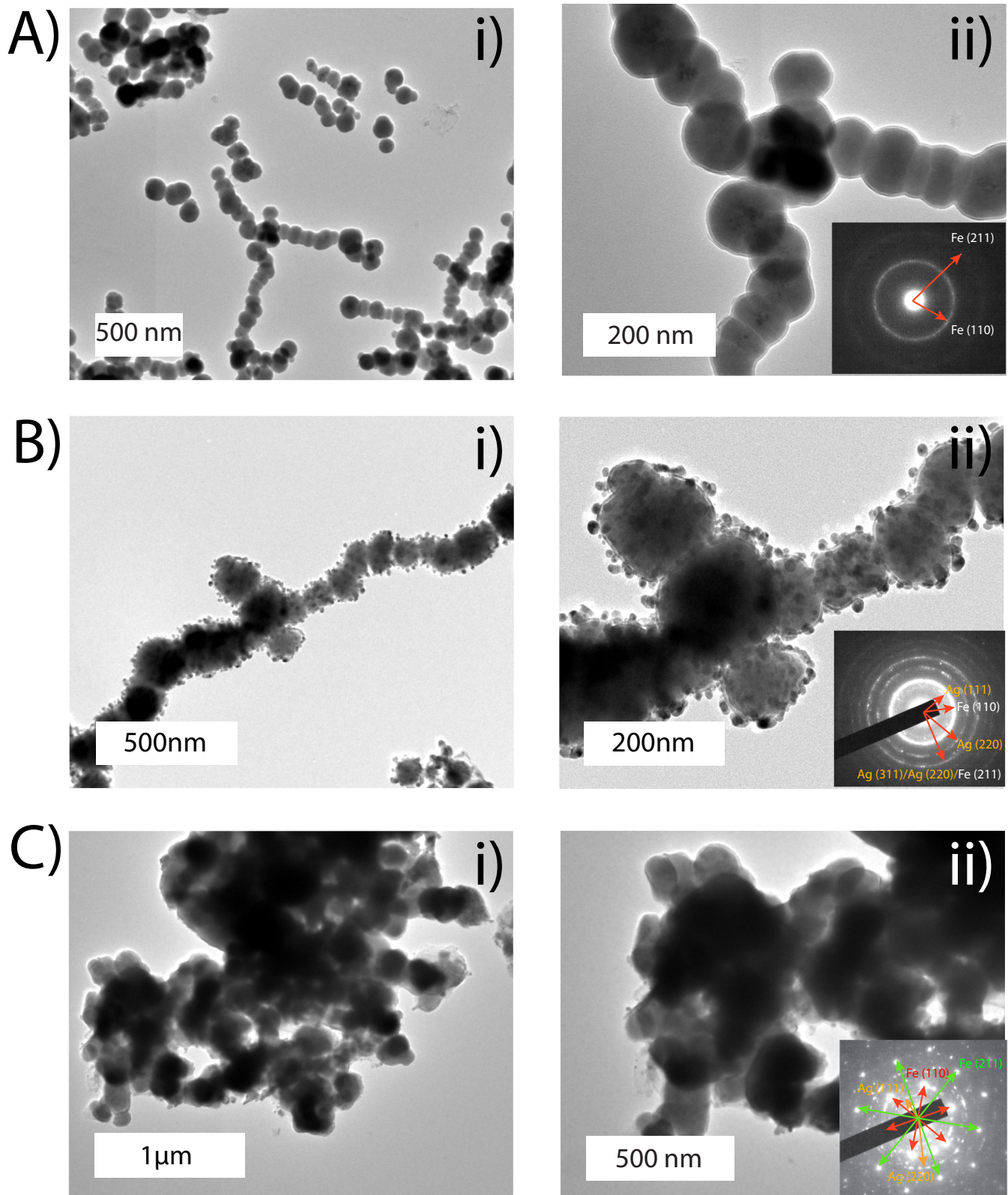


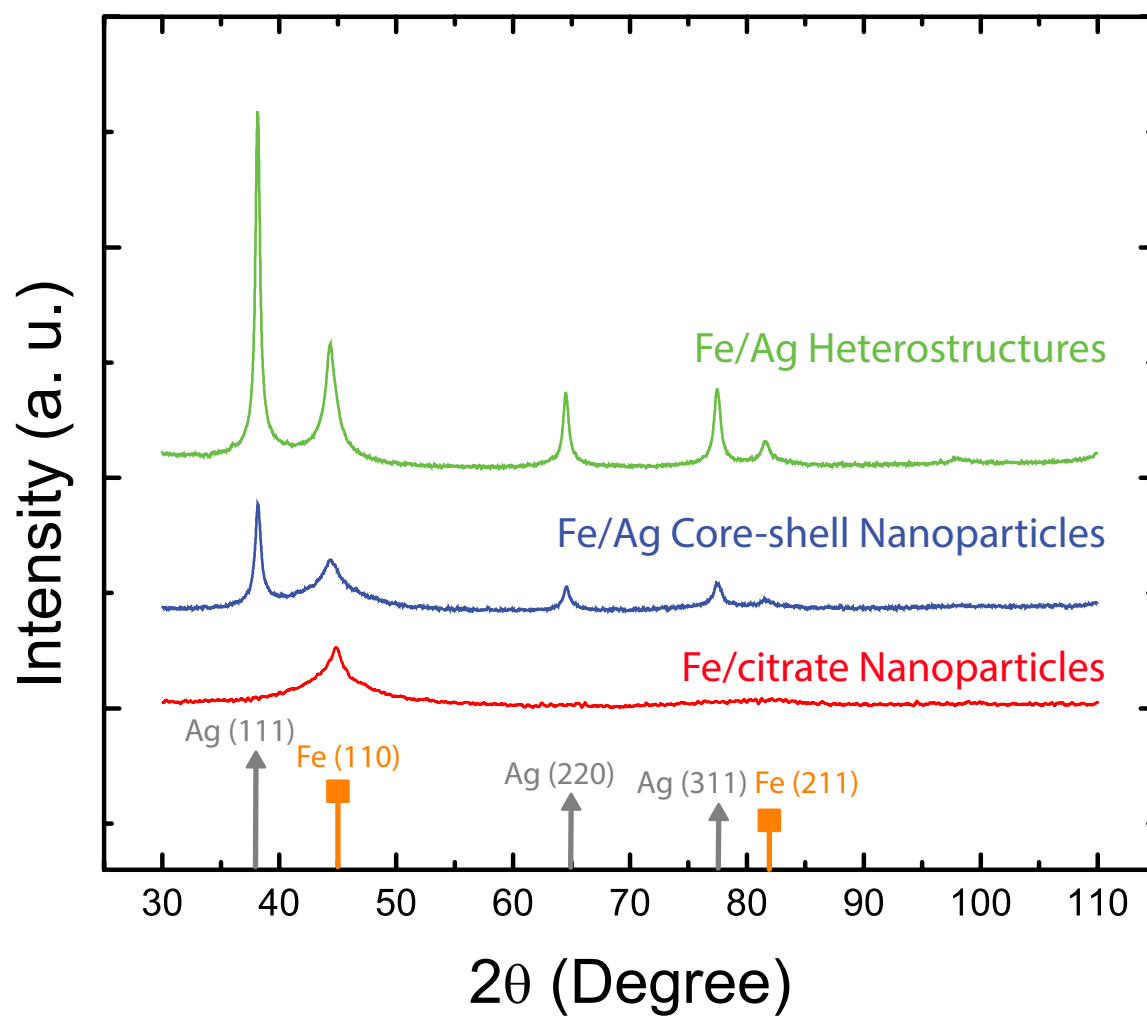
Figure 2:

Figure 3:

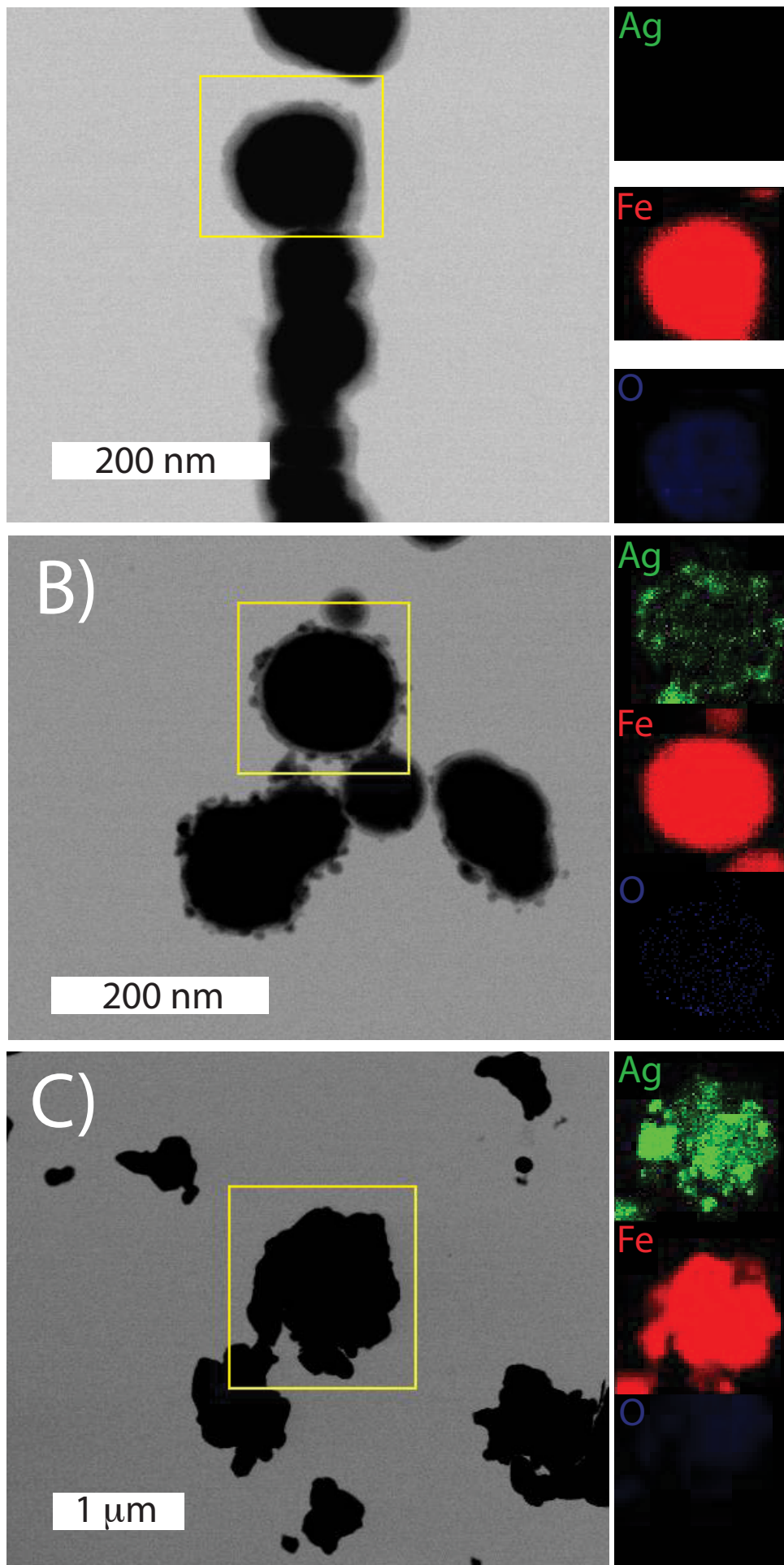


Figure 4:

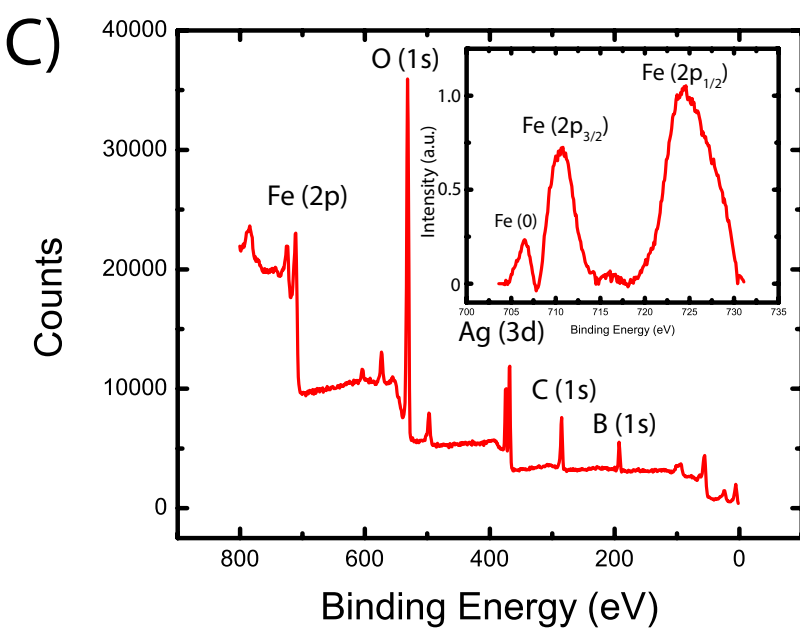
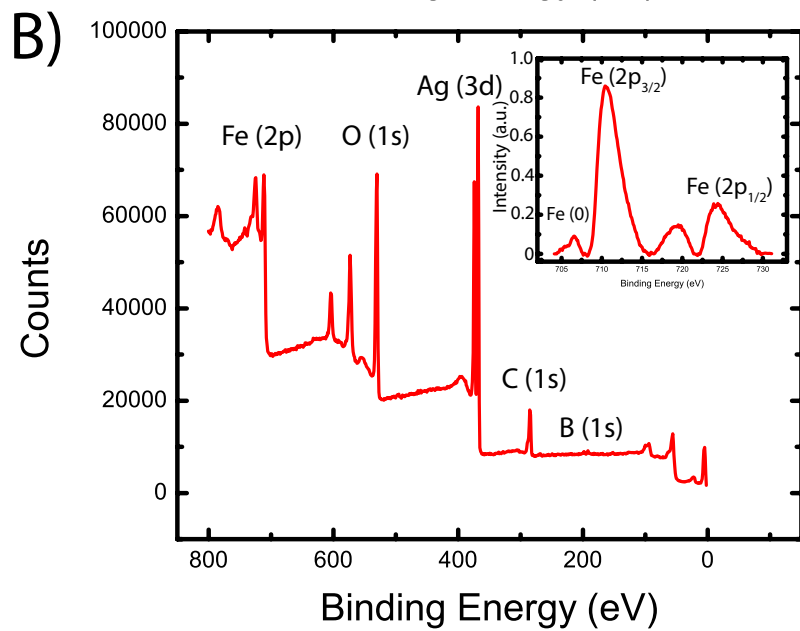
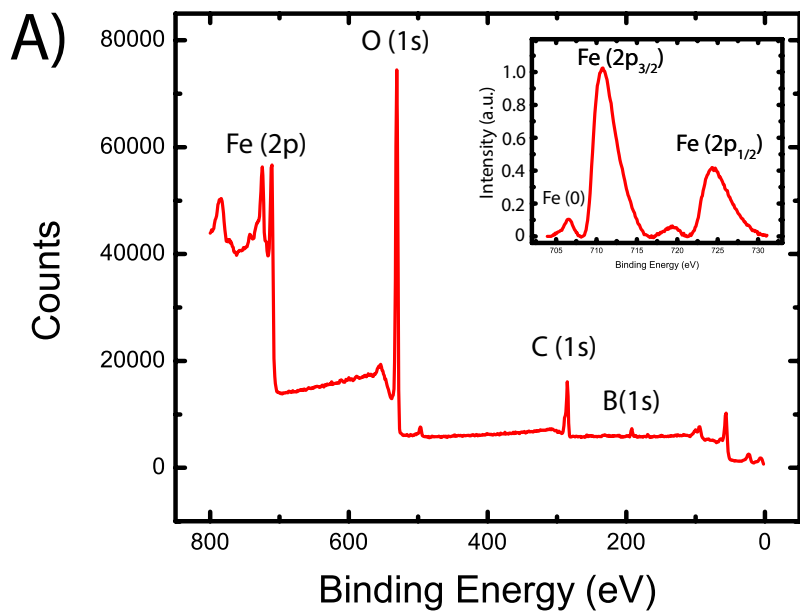


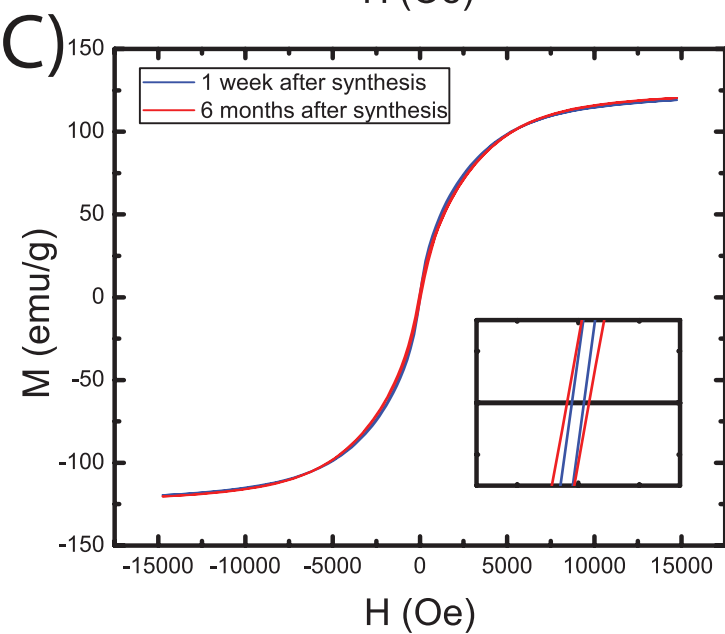
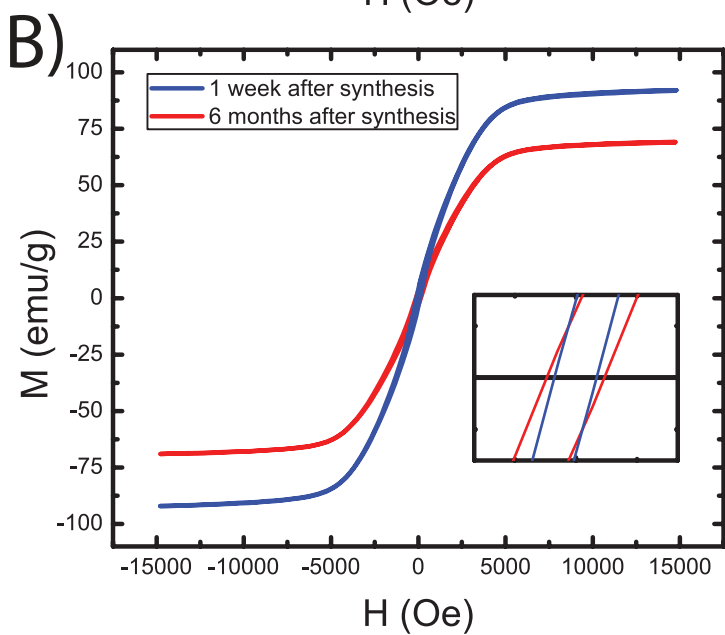
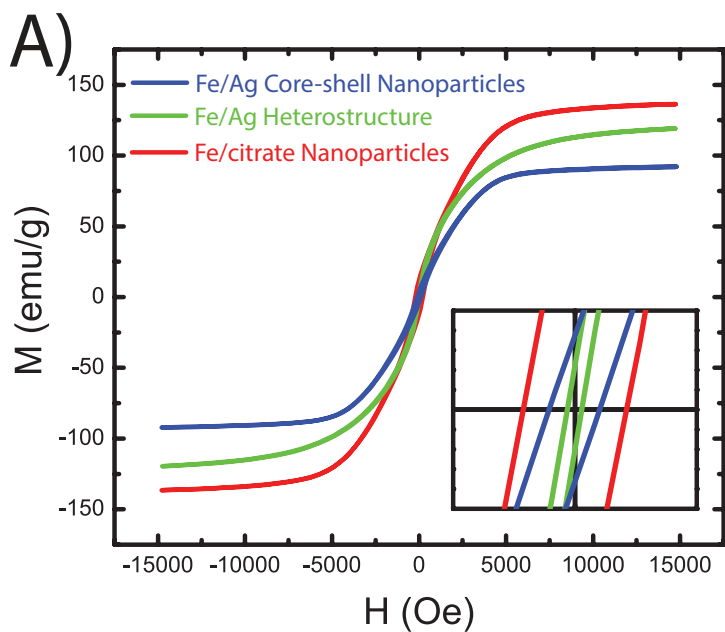
Figure 5:

Figure 6:

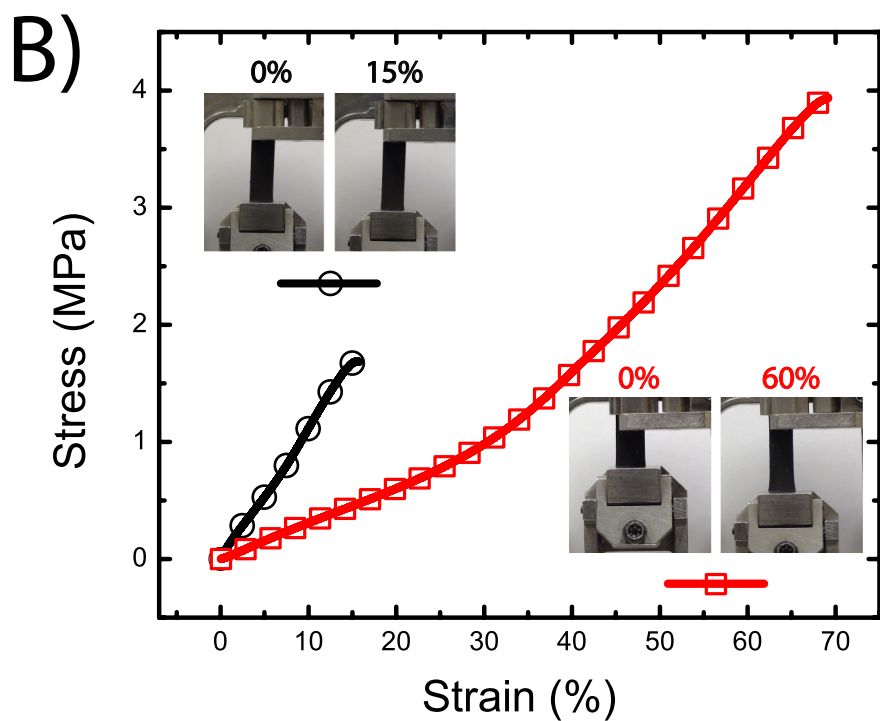
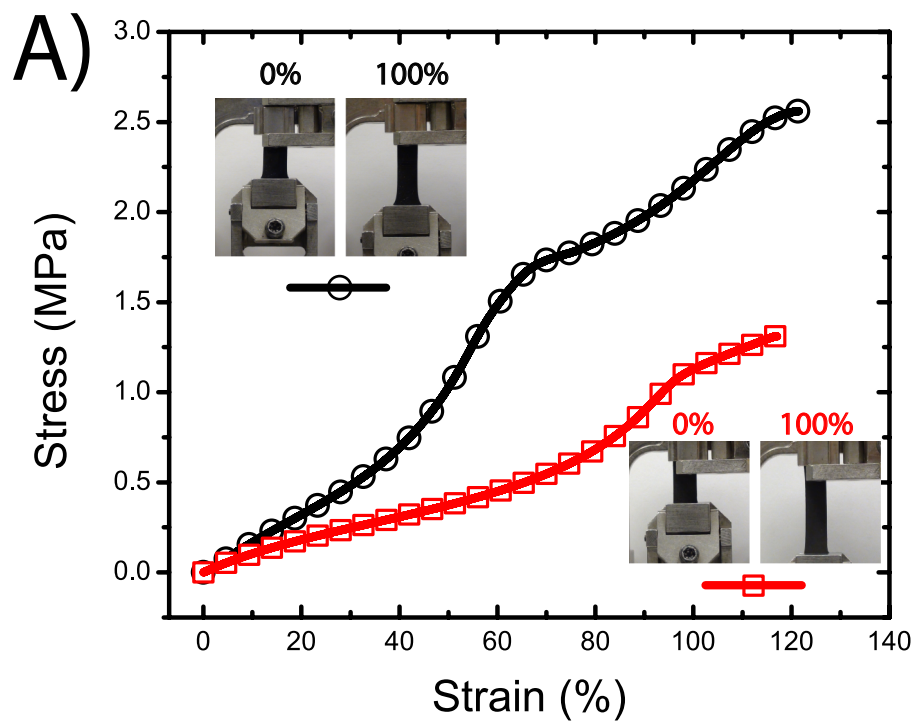
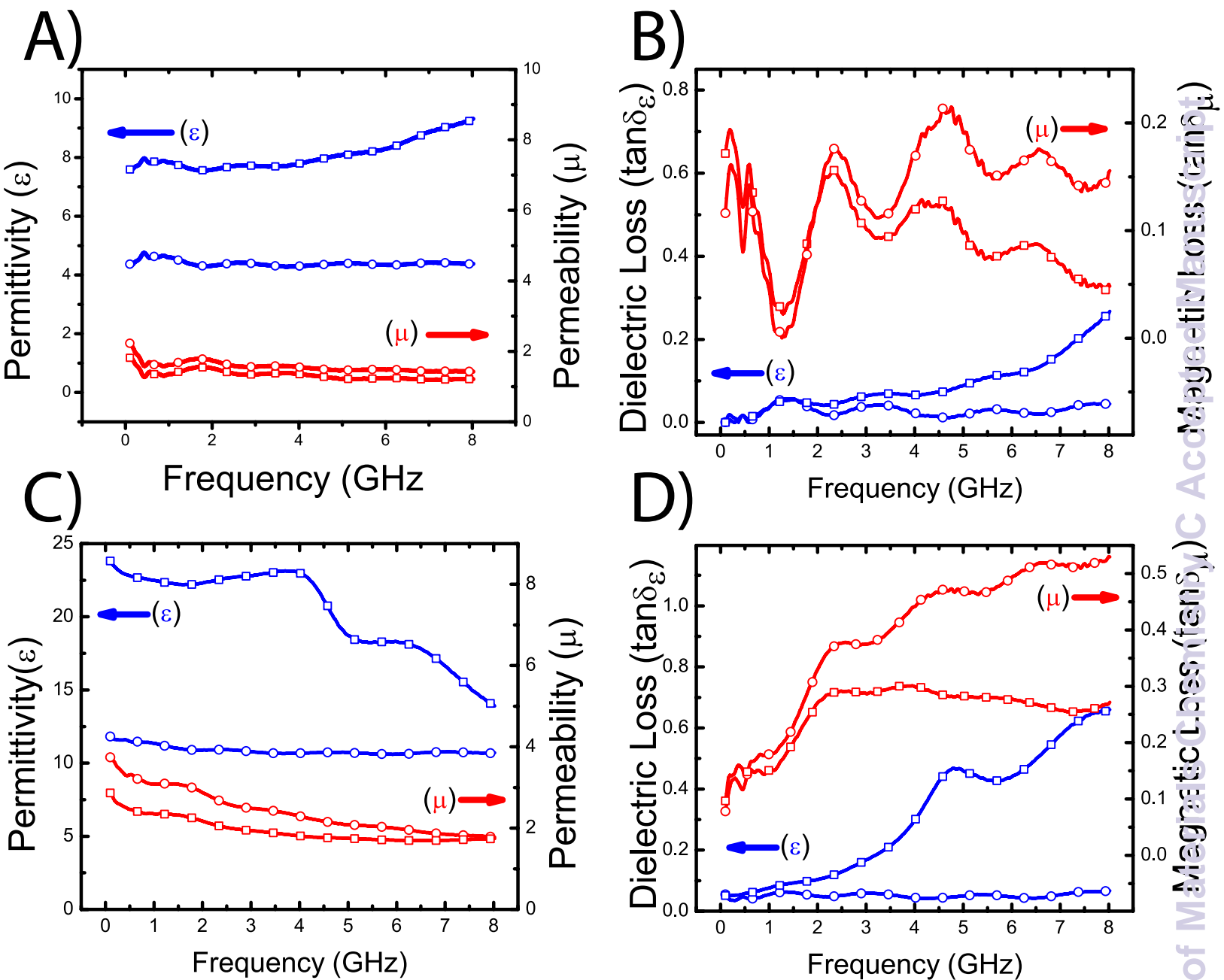


Figure 7:



The table of contents entry. Flexible magneto-dielectric composites with high permittivity, permeability and low loss are demonstrated and utilized to reduce the size radio frequency antennas.

Antenna Materials, Magnetic Nanoparticles, Polymer Composite, Magneto-dielectric Materials, Hybrid Materials

Mert Vural, Benjamin R. Crowgey, Leo C. Kempel and Peter Kofinas *

Nanostructured Flexible Magneto-dielectrics for Radio Frequency Applications

